Journal of Geophysical Research: Space Physics

RESEARCH ARTICLE
10.1029/2018JA025349

Special Section:
Dayside Magnetosphere Interaction

This article is a companion to Wang et al. (2018) https://doi.org/10.1029/2017JA024846.

Key Points:
- Both Pc 5 compressional and Alfvén waves are found to be generated by a foreshock transient
- Magnetospheric responses in the Pc 5 range are localized with clear dawn-dusk asymmetry
- The dawn-dusk asymmetry of wave power is consistent with the MLT location of the foreshock transient

Correspondence to:
Q. Shi and H. Zhang,
sqq@sdu.edu.cn;
hzhang14@alaska.edu

Citation:
Shen, X.-C., Shi, Q., Wang, B., Zhang, H., Hudson, M. K., Nishimura, Y., et al. (2018). Dayside magnetospheric and ionospheric responses to a foreshock transient on 25 June 2008: 1. FLR observed by satellite and ground-based magnetometers. *Journal of Geophysical Research: Space Physics*, *123*, 6335–6346. https://doi.org/10.1029/2018JA025349

Received 13 FEB 2018
Accepted 11 JUN 2018
Accepted article online 20 JUN 2018
Published online 15 AUG 2018

Dayside Magnetospheric and Ionospheric Responses to a Foreshock Transient on 25 June 2008: 1. FLR Observed by Satellite and Ground-Based Magnetometers

Xiao-Chen Shen[1,2,3], Quanqi Shi[1], Boyi Wang[3,4], Hui Zhang[1,5], Mary K. Hudson[2], Yukitoshi Nishimura[4,6], Michael D. Hartinger[7], Anmin Tian[1], Qiu-Gang Zong[8], I. J. Rae[9], and Alexander W. Degeling[1]

[1]Shandong Provincial Key Laboratory of Optical Astronomy and Solar-Terrestrial Environment, School of Space Science and Physics, Shandong University, Weihai, China, [2]High Altitude Observatory, National Center for Atmospheric Research, Boulder, CO, USA, [3]Department of Astronomy and Center for Space Sciences, Boston University, Boston, MA, USA, [4]Department of Atmospheric and Oceanic Sciences, University of California, Los Angeles, CA, USA, [5]Geophysical Institute, University of Alaska Fairbanks, Fairbanks, AK, USA, [6]Department of Electrical and Computer Engineering and Center for Space Sciences, Boston University, Boston, MA, USA, [7]Department of Electrical and Computer Engineering, Virginia Polytechnic Institute and State University, Blacksburg, VA, USA, [8]School of Earth and Space Sciences, Peking University, Beijing, China, [9]Mullard Space Science Laboratory, University College London, Dorking, UK

Abstract As one type of driver of magnetospheric Alfvén waves, foreshock transients have received less attention than, for example, the Kelvin-Helmholtz instability, discrete and broadband frequency solar wind dynamic pressure oscillations, and interplanetary shocks. Previous works show that foreshock transients can induce both Alfvén mode and compressional mode Pc 3–5 ULF waves inside the magnetosphere. However, to our knowledge, none of these reported Pc 3–5 waves, induced by foreshock transients, are proved to be localized in the magnetosphere. In this paper, using in situ and ground-based observations, we report the generation of localized magnetospheric compressional waves and field line resonances (FLRs) by a foreshock transient. Both the foreshock transient and Pc 5 ULF waves were found on the duskside; while on the morning side of the magnetosphere, no clear wave signatures were captured. Our results demonstrate that in addition to the global effects of foreshock transients on the magnetosphere reported earlier, foreshock transients can also generate localized magnetospheric responses in the Pc 5 range with clear dawn-dusk asymmetry. A suite of eight dayside spacecraft plus ground magnetometer measurements make possible the determination of the foreshock transient driver and dawn-dusk asymmetry of the magnetospheric response not previously reported with such a complete data set.

1. Introduction

Magnetospheric Pc 3–5 ULF waves are those continuous pulsations with period between 10 and 600 s (i.e., 1.7 to 100 mHz; Jacobs et al., 1964). Via wave-particle interactions, Pc 3–5 waves play an important role in the acceleration, transport, and loss processes of relativistic electrons near or within the outer radiation belt (e.g., Elkington et al., 1999; Hudson et al., 2000, 2017; Turner et al., 2012; Zong et al., 2009, 2012). For example, Zong et al. (2009) reported that electrons can be resonantly accelerated by the azimuthal electric field carried by poloidal modes. Elkington et al. (1999) and Hudson et al. (2000) studied electron acceleration that is caused by toroidal mode-driven inward radial transport and conserving the first adiabatic invariant. Additionally, outward radial transported electrons driven by toroidal modes could contribute to electron loss via magnetopause shadowing effects (e.g., Turner et al., 2012).

Generation mechanisms for Pc 3–5 ULF waves can be from external sources, such as solar wind dynamic pressure impulses (e.g., Claudepierre et al., 2010; Kepko et al., 2002; Sarris et al., 2010; Shi et al., 2013, 2014; Shen et al., 2015, 2017; Tan et al., 2004; Zong et al., 2009; Zhang et al., 2010), Kelvin-Helmholtz (K-H) waves at the magnetopause (Claudepierre et al., 2008; Pu & Kivelson, 1983), and foreshock transients (e.g., Eastwood et al., 2011; Hartinger et al., 2013; Zhao et al., 2017), as well as internal sources, like substorms (e.g., Hsu & McPherron, 2007; Olson & 17, 1999) and drift-bounce resonance with ring current ions (Southwood et al., 1969). Among

these generation mechanisms, foreshock transients, reported to drive ULF waves with amplitude comparable to that of shock-induced waves (Hartinger et al., 2013), have received less attention compared to the others.

Foreshock transients are kinetic processes generated in the ion foreshock region, where interplanetary magnetic fields (IMFs) are magnetically connected to the bow shock (e.g., Eastwood et al., 2005). In the foreshock, reflected ions from the bow shock toward the Sun can cause a number of instabilities, making contributions to the generation of ion foreshock transients, including hot flow anomalies (HFA; Xiao et al., 2015; Zhang et al., 2010), foreshock cavity, and foreshock bubbles (Turner et al., 2013). These foreshock transients could trigger magnetosheath high-speed jets (HSJs; Archer et al., 2012; Savin et al., 2012), magnetopause motion (e.g., Sibeck et al., 1999) and induce ULF waves inside the magnetosphere (e.g., Hartinger et al., 2013).

A few studies have reported that foreshock transients could induce magnetospheric Pc 3–5 waves (Eastwood et al., 2011; Hartinger et al., 2013; Zhao et al., 2017). Using Cluster, Rosetta, and ground observations, Eastwood et al. (2011) observed transient Pc 3 ULF waves induced by an HFA; Archer et al. (2015) studied the global effects of a foreshock bubble on the magnetosphere, including ULF wave activity; Hartinger et al. (2013) reported that Pc 5 ULF waves can be generated by HFAs, foreshock bubbles, and motion of the foreshock compressional boundary. Recently, Zhao et al. (2017) reported a global Pc 3 ULF wave event induced by an HFA, using Cluster and ground-based observations.

However, none of these reported Pc 3–5 waves, induced by foreshock transients, are proved to be localized in the magnetosphere. Additionally, no Pc 5 standing Alfvén waves, which are mainly regarded as fundamental field line resonances (FLRs; e.g., Chen & Hasegawa, 1974; Claudepierre et al., 2010), have been reported to be driven by foreshock transients.

In this paper, we report on the generation of localized compressional and standing Alfvén waves by a foreshock transient. During this event, Pc 5 compressional waves were first observed near noon, then propagated to the afternoon sector based on in situ and ground observations. FLRs (standing Alfvén waves) were excited in the afternoon sector, based on in situ observations, while on the morning side of the magnetosphere, no clear ULF wave signatures were captured by satellites or ground magnetometers.

The paper is organized as follows: section 2 introduces the data sets that have been used in this work. Section 3 presents the observations of the solar wind, magnetosheath conditions, and ULF waves in the dayside magnetosphere. Section 4 discusses the wave energy source and FLRs. A summary is given in the last section. In a companion paper, Wang et al. (2018 hereinafter Paper 2) presents 2-D evolution of the magnetosphere and ionosphere deduced from optical observations.

2. Data Set

The solar wind, IMF parameters, and magnetospheric measurements used in this paper are obtained from the Time History of Events and Macroscale Interactions During Substorms (THEMIS) mission (Angelopoulos, 2008), which consists of five identical probes (THA, THB, THC, THD, and THE). Each probe is equipped with a fluxgate magnetometer (Auster et al., 2008), which provides magnetic field data and an electrostatic analyzer (McFadden et al., 2008), which provides thermal (5 eV to 25 keV) ion and electron data. We use 3-s resolution spin-fit data from those instruments.

We have also used supporting data from Geostationary Operational Environmental Satellite spacecraft (G10, G11, and G12) and ground-based magnetometers (KIAN, FSMI, RBAY, CDRT, ATU, STF, NAQ, SCO, and BJN stations).

Figure 1 shows the locations of the satellites in (left) the GSE *x*-*y* plane and (right) *x*-*z* plane. During 1530 to 1600 UT, THB and THC satellites were located in the solar wind, monitoring solar wind plasma and IMF conditions. THA was situated most often in the magnetosphere and made intermittent passages into the magnetosheath. THD and THE were located in the duskside magnetosphere, observing wave signatures. G10 and G12 were in the dayside magnetosphere near local noon. G11 was located on the dawnside of the magnetosphere. The black curve indicates the location of the magnetopause estimated from the Shue et al. (1998) model.

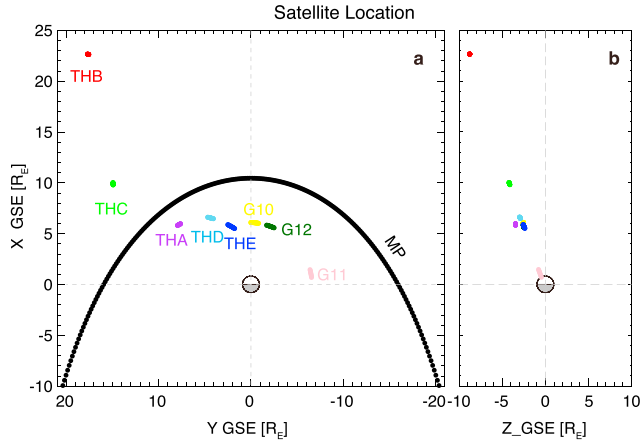

Figure 1. Satellites traces during 1530 to 1600 UT on 25 June 2008 in GSE coordinates. (a) *x*-*y* plane and (b) *x*-*z* plane. The black curve in the *x*-*y* plane indicates the magnetopause Shue et al. (1998) model at $z = 0$. The Sun is to the top.

3. Observations

3.1. Solar Wind and Magnetosheath Conditions

Figure 2 shows the solar wind conditions observed by (left) THB and (right) THC satellites. THC (X_{GSE} is approximately 10.0 R_E) was located closer to the Earth than THB (X_{GSE} is approximately 22.7 R_E). Figures 2a–2e show THB observations of IMF, magnetic field strength, ion density, ion velocity, and ion energy flux, respectively. During ~1536 UT to ~1541 UT, depletions in magnetic field and density were identified. At the same time, an enhancement in the flux of high-energy ions, ~1–10 keV, can be seen from the ion energy flux spectrum.

Figures 2f–2l show THC observations of IMF, ion density, ion velocity *x* component, dynamic pressure, ion temperature, electron energy flux, and ion energy flux, respectively. During ~1537 UT to ~1545 UT, depletions in magnetic field, density, and velocity were identified. Meanwhile, plasma temperature was elevated. A distribution of hot plasma can be seen from the ion energy flux spectrum. Yellow-shaded areas mark similar phenomena observed by the two satellites. Comparing the THB and THC observations, one can find that these

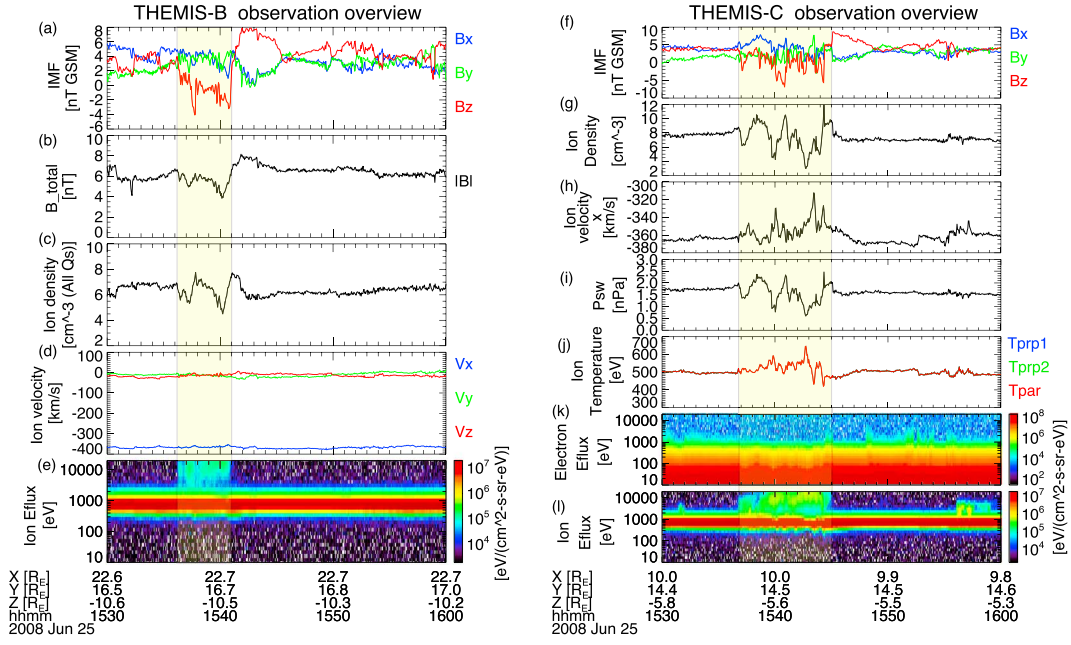

Figure 2. THB and THC observations overview. THB observations of (a) IMF, (b) magnetic field magnitude, (c) ion density, (d) ion velocity in GSM coordinates, and (e) ion energy flux spectrum, respectively. THC observations of (f) IMF, (g) ion density, (h) ion velocity, (i) solar wind dynamic pressure, (j) ion temperature, (k) electron energy flux, and (l) ion energy flux, respectively.

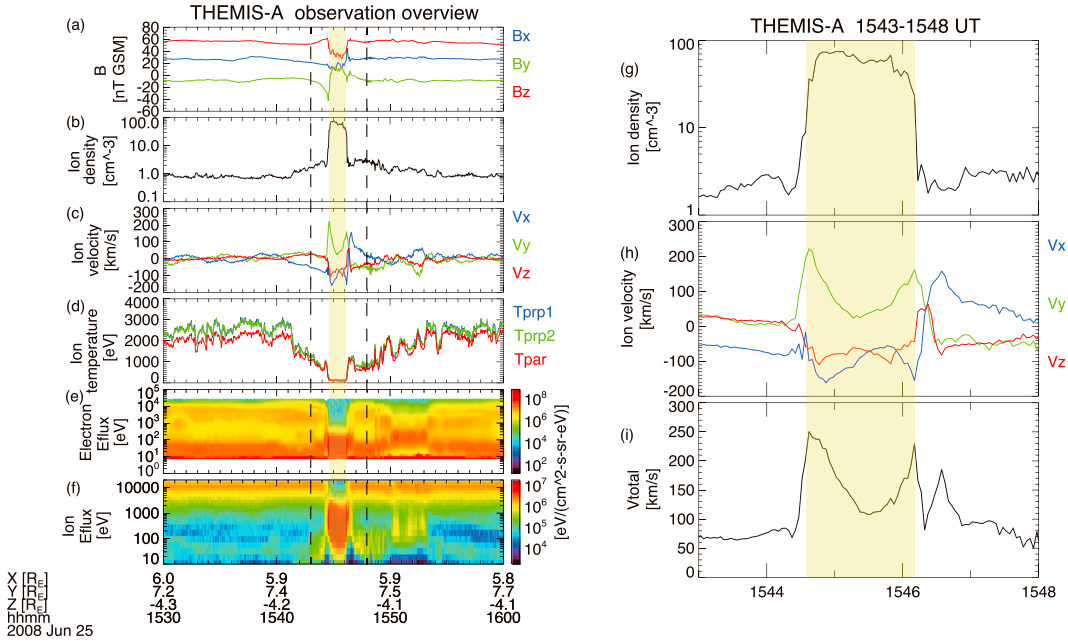

Figure 3. THA observations of (a) magnetic field components, (b) ion density, (c) ion velocity, (d) ion temperature, (e) electron energy flux, and (f) ion energy flux from 1530 to 1600 UT and (g) ion density, (h) ion velocity, and (i) total velocity from 1543 to 1548 UT. Two black dashed lines in the left plot present the time period that has been zoomed in as shown in the right of the figure. Yellow-shaded area indicates magnetosheath region.

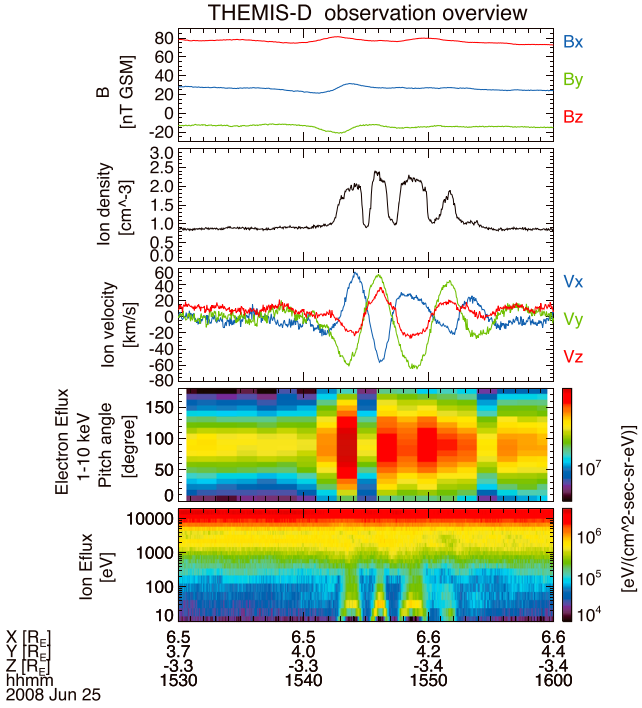

Figure 4. THD observations overview. From top to bottom shows the THD observations of magnetic field components, ion density, ion velocity in GSM coordinates, pitch angle distribution of 1–10 keV electrons, and ion energy flux, respectively.

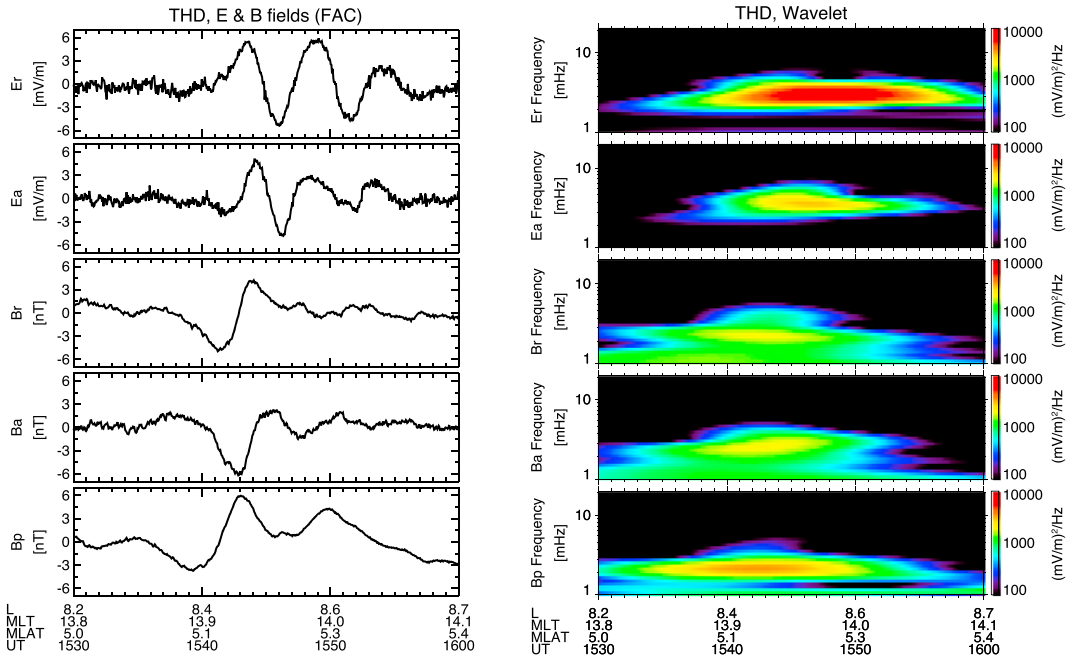

Figure 5. THD observations of the ULF waves. (left) Electric and magnetic fields measured from THD in field-aligned coordinates (FAC). (right) Wavelet analysis of the electric and magnetic fields components in FAC.

features are similar but more clear at THC, which is closer to the bow shock region. Both of them observed depletions in magnetic field and ion density while ion temperature was elevated (not shown for THB). Energetic ions (~1–10 keV) have also been identified by the two satellites during the shaded time period. These characteristics indicate the possibility that THC and THB observed a proto-hot flow anomaly (proto-HFA) event close to the bow shock region (Zhang et al., 2010) or a foreshock cavity. In other words, a foreshock transient event was observed during that time by THB and THC.

Figure 3 shows the THA observations near the magnetopause. Figures 3a–3f show magnetic field (GSM coordinates), ion density, ion velocity (GSM coordinates), ion temperature, electron energy flux, and ion energy flux, respectively. The region between two dashed black lines shows the crossing from the magnetosphere (characterized by low density, high magnetic field magnitude, low ion velocity, and high ion temperature) to the magnetosheath (characterized by high density, low magnetic field magnitude, high ion velocity, low ion temperature, and clear ion energy flux distribution around 1keV) at ~1544 UT, then back to the magnetosphere at ~1546 UT. The yellow-shaded time period shows that THA was located in the magnetosheath. Figures 3g–3i zoom in to the time period of interest from 1543 to 1548 UT indicated by the two dashed lines in Figure 3a. From top to bottom, panels show the ion density, ion velocity components in GSM coordinates, and total velocity, respectively. The total velocity in the sheath (yellow-shaded area) varies from ~110 km/s to ~250 km/s, suggesting that a magnetosheath high-speed flow may exist. This is consistent with Table 2 of Dmitriev and Suvorova (2015), where this time period is listed as a magnetosheath high-speed flow event.

3.2. Satellite Observations of ULF Waves

Figure 4 shows (from top to bottom) the magnetic field, ion density, ion velocity, electron energy flux, and ion energy flux from THD observations. One can find that after ~1541 UT, disturbances were observed in the magnetic field, ion density, ion velocity, electron energy flux, and the ion energy flux. Ion velocity shows nearly monochromatic wave signatures. The 1–10 keV electron flux pitch angle distribution shows 90° flux enhancements that vary with period close to the wave period observed in the ion velocity, indicating the existence of wave-particle interactions. Ion density shows modulations with double the frequency of the ion velocity waves, which could be caused by low-energy ions (≤100 eV) accelerated locally by the electric field (no matter in which direction the acceleration is perpendicular to the background magnetic field), seen in the bottom panel of Figure 4.

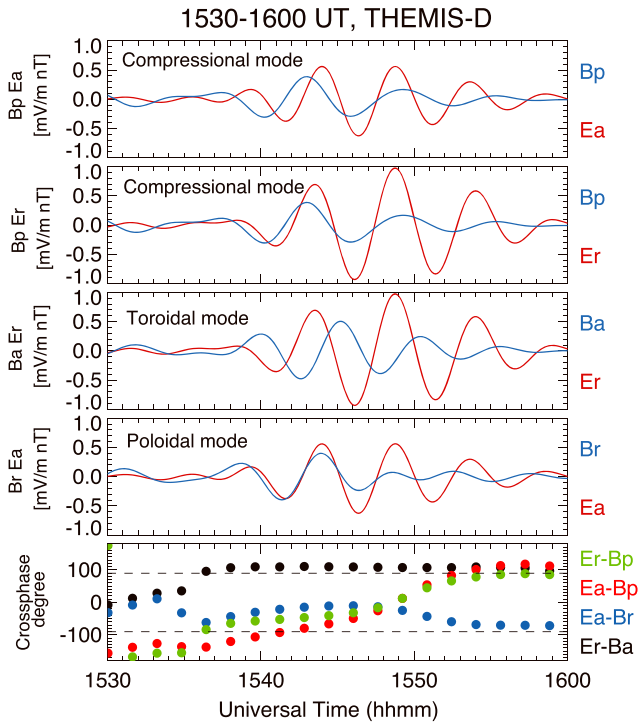

Figure 6. Wave modes and phase difference analysis. Top four panels show the 3.1 to 3.5 mHz filtered electric and magnetic fields associated with compressional mode, compressional mode, toroidal mode, and poloidal mode, respectively. Last panel shows the phase differences between the electric and magnetic fields for these modes near 3.3 mHz. Dashed lines in the last panel mark ±90°.

Figure 5 shows the (left) electric and magnetic fields from THD observations in field-aligned coordinate (FAC) system (e.g., Hartinger et al., 2011; Takahashi et al., 1990) and (right) the wavelet analysis of them. In the FAC, *a* points in the azimuthal direction, *r* points in the radial direction, and *p* is parallel to the field line. The amplitude of electric and magnetic fields reached 6 mV/m and 6 nT, respectively, which is comparable to that of shock-induced ULF waves (Walker et al., 1982; Zong et al., 2009). Narrow band frequency distribution, 2 to 4 mHz, was captured from wavelet analysis of the electric and magnetic fields. According to Jacobs et al.'s (1964) classification, the wave belongs to the Pc 5 ULF wave category. The wave power of E_r is stronger than that of E_a.

Figure 6 shows the phase difference analysis between the electric and magnetic fields obtained from the THD satellite. The top four panels show the 3.1- to 3.5-mHz filtered electric and magnetic field components for the two compressional modes, the toroidal mode, and the poloidal mode. The bottom panel shows the phase difference between the electric and magnetic field components near 3.3 mHz. Time window we applied to calculate the phase differences is 768 s (256 points multiple 3-s/point time resolution) with 96 s (32 points) shifted time window. Therefore, time resolution of the calculated phase difference is 96 s. Black dots represent the phase difference for the toroidal mode; blue dots represent the phase difference for the poloidal mode; green and red dots represent the phase differences for two compressional modes. Dashed black vertical lines in the bottom panel of Figure 6 mark ±90°. The toroidal mode shows near 90° phase difference, indicating that standing Alfvén waves are formed along the magnetic field lines (Tamao, 1965). Electric field is leading magnetic field by +90° phase difference in the north of magnetic equator (about 5.2° magnetic latitude, MLAT). This is a feature of fundamental mode (or odd harmonics modes), instead of second harmonic mode, which should show −90° in the north of the magnetic equator (Takahashi et al., 2015).

Figure 7 shows the THE observations of electric and magnetic fields in FAC. During 1530 to 1600, THE was closer to the Earth than THD. Even though the amplitude was weaker than that from THD observations, one could still find distinct wave signatures in the magnetic field (amplitude: less than 3 nT) from ~1540 UT. The electric field did not show clear wave signatures, which may be due to the fact that the THE satellite was

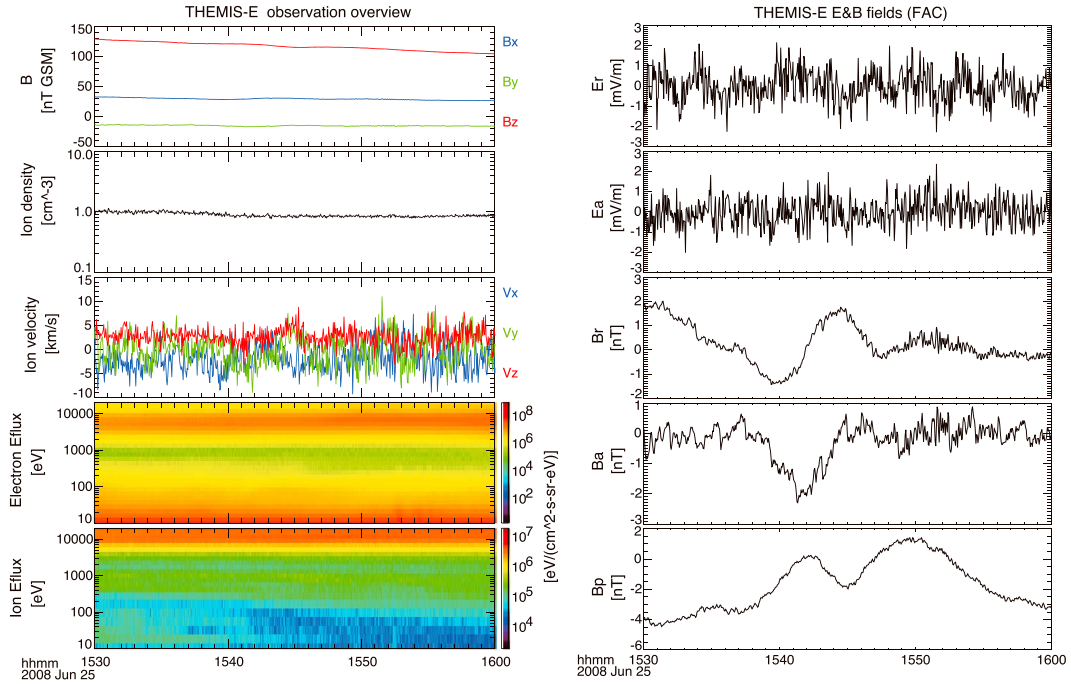

Figure 7. (left) THE observations of magnetic field, ion density, ion velocity, electron energy flux spectrum, and ion energy flux spectrum. (right) Electric and magnetic fields measured from THE in FAC.

away from the FLR region. During 1540 to 1550 UT, THD was located at $L = 8.4–8.6$ and THE was located at $L = 6.6–6.8$.

Figure 8 shows the magnetic field components measured by G11, G12, G10, THE, and THD (note that the sequence of these satellites is based on the MLT of these satellites from dawnside to duskside of the magnetosphere). The top panel presents the dynamic pressure changes monitored by THC upstream of the bow shock for reference. Three columns, from left to right, show the radial, azimuthal, and parallel components of the magnetic field, respectively. G11, located the most dawnward of the five spacecraft inside the magnetopause in Figure 1, did not observe clear wave signatures during the event. G12, G10, and THE were close to noon and observed strong Bp variations, which is associated with compressional waves. On the duskside of the magnetosphere, THD observed strong Br and Ba variations, which are associated with Alfvén waves, as well as Bp variations. From the stack plot, one can find that waves were first observed at G12 satellite, which is located at about 10.3 MLT, then propagating duskward and observed by G10, THE, and THD, respectively, at 11.3, 12.2, and 14.0 MLT. The speed of wave is 0.43 to 0.65 hr MLT per minute (79 to 120 km/s at $L = 6.6$ in the equator). Please see Figure 4 and figure caption of paper 2 for details. This speed is much lower than local magnetosonic wave speed, which should be in the order of 1,000 km/s with plasma and magnetic field parameters from THD, but close to the azimuthally propagating speed of the foreshock transient, inferred from the propagating speed of the discontinuity in the solar wind, please see Table 1 in the Paper 2. It is suggested that fast mode waves launched by the small-scale foreshock transient may damp fast and not propagate very far. The fast mode waves observed by satellites should be launched by the foreshock transient at the magnetopause at different MLT.

3.3. Ground Observations of ULF Wave

Figure 9 shows the magnetic fields from ground-based magnetometers. From top to bottom, panels show magnetic fields observed from different ground stations ranging from ~3.04 to 17.39 MLT (MLT was calculated at 1540 UT) with magnetic latitude (MLAT) close to 70°. Magnetic field vectors are shown in HDZ coordinates, where the H direction points to magnetic north, D is along magnetic east, and Z points vertically downward. Clear wave oscillations can be seen in the ATU, STF, NAQ, and SCO stations (from noon to afternoon sector). On the morning side, there is no obvious wave signature compared to the afternoon sector.

The wave was first observed at the ATU station (MLT = 12.75) near ~1535 UT, then propagated to the afternoon sector. It should be noted that there is a time delay of the observation of wave signatures at STF station.

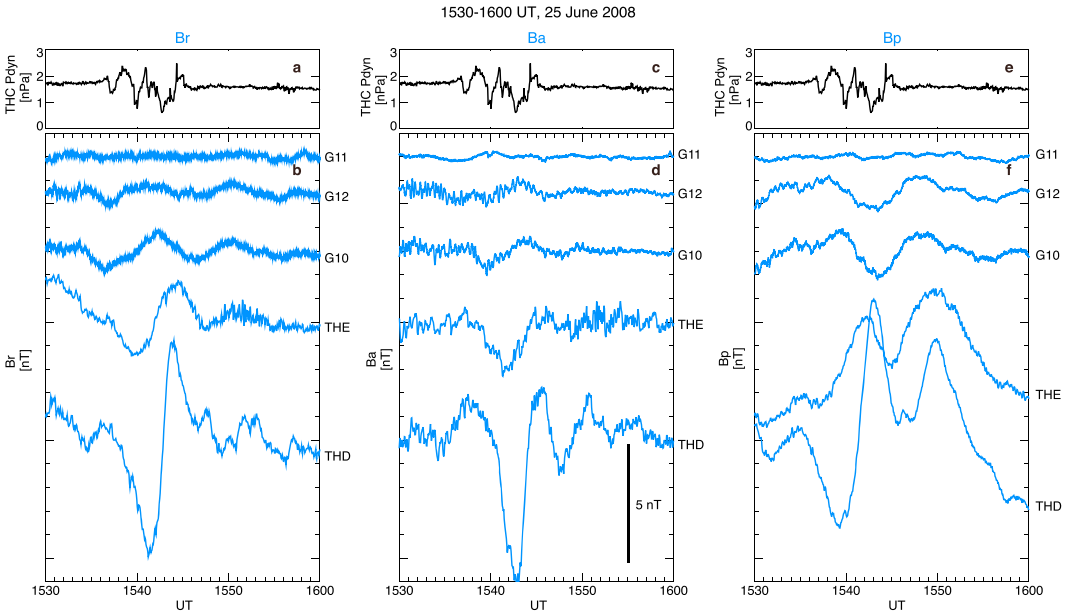

Figure 8. Stack plot of satellite observations of magnetic field components in FAC system. (a, c, e) Solar wind dynamic pressure measured by THC. (b) Radial, (d) azimuthal, and (f) parallel components of magnetic field measured by G11, G12, G10, THE, and THD. Note that the sequence of these satellites in the bottom panel are based on the MLT, from dawn to dusk side of the magnetosphere. MLT = magnetic local time.

For this event, scale of the upstream disturbance is small (comparing to a shock), usually less than several Earth radii and is propagating duskward with a speed of 0.5-hr local time per minute. The fast mode waves observed at different L and MLT may be lauched at the magnetopause with different MLT at different time by the foreshock transient. This could be a possible reason of causing the delay at STF station. It took about ~13 min elapsed for the wave to propagate from the ATU station (MLT = 12.75) to the BJN station (MLT = 17.39). Considering the fact that MLT of two stations changed 0.22 hr during 13 min, the wave is eastward (duskward) propagating with a speed of about 0.56-hr local time per minute, which is consistent with satellite observations. As mentioned above, this speed is suggested to be associated with the azimuthal propagation of the foreshock transient.

4. Discussion

On 25 June 2008, a foreshock transient was identified by THB and THC satellites in the duskside outside the bow shock at ~1536 and ~1537 UT, respectively. THA was located in the magnetosphere near the magnetopause at that time and observed inward and outward motion of the magnetopause during ~1544 to ~1546 UT. Around ~1535 to ~1600 UT, distinct wave signatures were captured by THD, THE, G10, and G12 satellites in the noon to afternoon sector of the magnetosphere. Furthermore, standing toroidal mode waves at ~3.3 mHz were observed by THD.

4.1. Wave Energy Source

During this event, geomagnetic activity was low ($AE \leq 50$ nT, $Kp \leq 3$, $Dst \sim -2$ nT). The solar wind speed is less than 400 km/s, which is a normal solar wind speed (Hapgood et al., 1991) and of low possibility to induce K-H waves at the dayside flank magnetopause (Ogilvie & Fitzenreiter, 1989).

From THB and THC observations (see Figure 2), a foreshock transient occurred from ~1536 UT to 1537 UT, accompanied with solar wind dynamic pressure perturbations. THA observed inward and outward motion of the magnetopause at ~1544 UT and ~1546 UT, respectively; please see Figure 3. The magnetopause motions may be modulated by the solar wind dynamic pressure perturbations imbedded in the foreshock transient (see Figure 2). While THA traveled into the magnetosheath, a high-speed sheath jet was observed. The jet traveled mostly along the magnetopause (inferred from comparable V_X and V_Y, see panel two in the right plot of Figure 3). We suggest that the magnetopause motions were induced by the foreshock transient in order to maintain pressure balance. The observation of magnetopause motions is later than expected

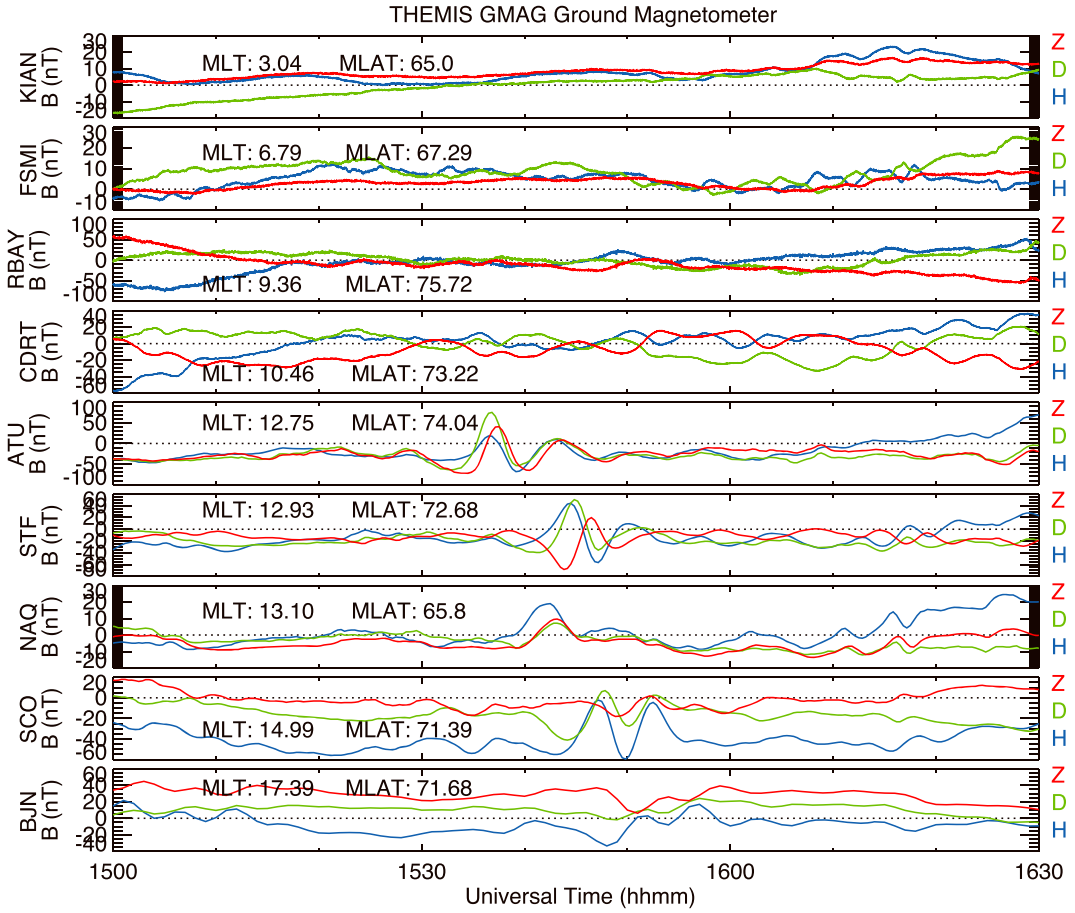

Figure 9. Geomagnetic fields obtained from THEMIS GMAG ground magnetometers. MLT and MLAT (calculated at 1540 UT) for each station have been labeled on each panel. THEMIS = Time History of Events and Macroscale Interactions During Substorms; MLT = magnetic local time; MLAT = magnetic latitude.

(several minutes). Paper 2 shows that the foreshock transient measured by THB and THC is associated with IMF discontinuities. Based on the timing, the discontinuities are tilted dawnward and swept through the magnetosheath duskward. The discontinuity propagation explains the timing and propagation of ULF signals from dawn to dusk by the foreshock transient.

4.2. Wave Distributions

ULF oscillations were observed at G10 and G12 near noon MLT at ~1535 UT (see Figure 8). THD and THE in the afternoon sector observed a corresponding wave signature around 1541 UT (Figures 4 and 7). Ground magnetometer observations show coincidental observations at station ATU at 12.75 MLT around ~1535 UT. Stations STF and NAQ at ~ 13 MLT observed the waves at ~1540 UT. Station BJN in the duskside observed the waves at ~1548 UT.

The compressional mode wave frequency observed by THD was 2–4 mHz. The magnetic field fluctuation observed by THE, G10, and G12 deeper near the noon MLT was ~2 mHz. Additionally, ground magnetometer station observations of the magnetic fields show that the frequency is ~2–4 mHz from ~65° to ~74° magnetic latitude.

The satellites and ground observations show that compressional mode waves were launched near noon by the ion foreshock disturbance via pressure balance at the magnetopause. Then these waves spread eastward to the afternoon sector, while in the morning sector, there are no obvious wave signatures captured by satellite or ground magnetometer. These observations lead to a suggestion that compressional waves were excited most strongly when the ion foreshock disturbance moved into the afternoon sector, as indicated by THB/THC observations. Additionally, a ~3.3 mHz toroidal mode standing Alfvén wave was driven at the location of THD. With assumptions that the magnetic field is dipolar (Degeling et al., 2010) and density is a power law

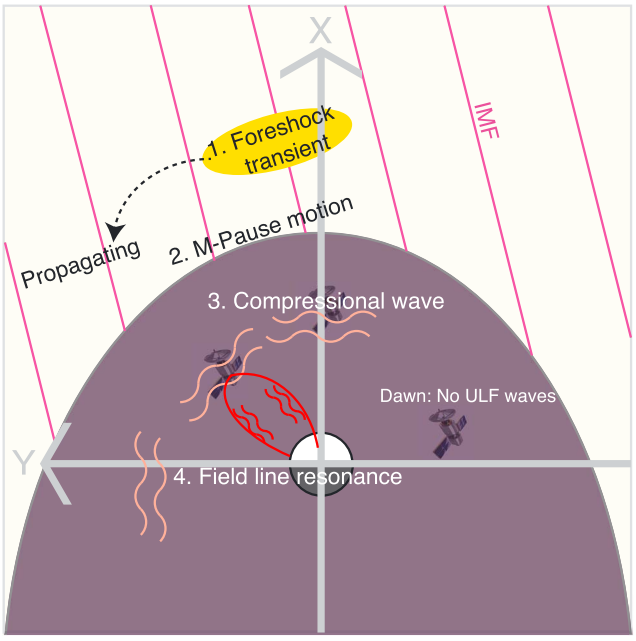

Figure 10. Schematic diagram showing the responses of the magnetosphere to the foreshock transient event on 25 June 2008.

distribution (Denton et al., 2006), with power law index equals 4.0, the eigenfrequency of the field line near THD was calculated to be 4.3 mHz (poloidal mode) and 5.1 mHz (toroidal mode); please see Rankin et al. (2005) for calculation method. The calculated eigenfrequency of the field line is close to the observed 3.3 mHz field line resonance, and ratios of observed to calculated frequencies of approximately 0.7 are reasonable for distorted, nondipolar field geometries (e.g., Berube et al., 2006). As mentioned in section 3.2, the wave mode should not be a second harmonic mode due to the +90° phase difference between electric and magnetic fields in the north of magnetic equator. Thus, it is suggested to be a fundamental mode toroidal wave.

Wave mode number m is estimated using ground magnetometer measurements. The wave number $m = \delta\phi/\delta\lambda$ (Sarris et al., 2009), where $\delta\phi$ is the phase difference of the H magnetic field component and $\delta\lambda$ represents the longitudinal difference between the two stations. Even a small separation in geomagnetic latitude between two stations may result in considerable error (Sarris et al., 2013). To minimize error, we choose stations SCO (MLT: 14.99, MLAT: 71.39) and BJN (MLT: 17.39, MLAT: 71.68) with small difference in geomagnetic latitudes. The parameter $\delta\phi$ is calculated to be ~291° and $\delta\lambda$ is 36° for the two stations. Thus, the wave mode number m is ~8. However, if these waves are propagated from different locations of the magnetopause at different times, the calculated wave mode number may not be trustable.

Figure 10 shows the schematic diagram of a foreshock transient accompanied with dynamic pressure changes impacting the magnetosphere, making the magnetopause move inward and outward. Then compressional mode waves are launched at the magnetopause. These waves are propagated from noonside to the afternoon side of the magnetosphere. At the location where the compressional mode frequency is harmonically matched to the FLR frequency, FLRs will be excited (Hughes, 2013; Lee & Lysak, 1989). The magnetic field direction was obtained based on the 5-min average of the magnetic field before the THC observation of foreshock transients, please see Figure 2f.

5. Summary

In this paper, we studied a FLR event on 25 June 2017 from satellite and ground magnetometer observations. In the upstream region, a foreshock transient was observed by THB and THC. THA, near the magnetopause, monitored an inward and outward motion of the magnetopause. In the dayside magnetosphere, G10, G11, THD, and THE observed Pc 5 ULF wave activity. The amplitude of electric and magnetic fields observed by THD reached 6 mV/m and 6 nT, respectively. On the morning side, no clear wave signatures were captured based on space and ground observations.

Radial component electric field is leading azimuthal component magnetic field by 90° phase difference in the north of the magnetic equator, indicating that fundamental (or odd harmonics) toroidal mode standing Alfvén waves were formed along the field lines. These features suggest that FLRs may be driven by compressional waves at a certain L shell (location of THD) where the compressional wave and FLRs are harmonically matched to each other (Hughes, 2013; Lee & Lysak, 1989). The compressional wave itself is induced by the ion foreshock transient via pressure balance at the magnetopause. Moreover, a theoretical approach of eigenfrequency of field line resonance confirms that the driven waves are fundamental mode.

These results show that magnetospheric compressional waves and FLRs induced by foreshock transients can be localized in the same or close MLT sector as that of foreshock transients. This demonstrates that, in addition to the global effects of foreshock transients on the magnetosphere revealed by earlier studies, foreshock transients can also generate localized magnetospheric response in the Pc 5 range. Longitudinal localization of ULF wave power is often neglected in the analysis of ULF wave effects on radiation belt electrons (Hao et al., 2017; Rae et al., 2018) and warrants further investigation.

Acknowledgments
We acknowledge NASA contract NAS5-02099 and V. Angelopoulos for use of data from the THEMIS Mission (http://themis.ssl.berkeley.edu/data/themis/). Specifically, C. W. Carlson and J. P. McFadden for use of ESA data, K. H. Glassmeier, U. Auster, and W. Baumjohann for the use of FGM data provided under the lead of the Technical University of Braunschweig, S. Mende and C. T. Russell for use of the GMAG data and NSF for support through grant AGS-1004814, TromsØ Geophysical Observatory, University of TromsØ, Norway for use of the Greenland and Norway magnetometer data, Erik Steinmetz, Augsburg College for the use of GMAG data. NOAA GOES data are obtained from the website: https://cdaweb.sci.gsfc.nasa.gov/index.html/. This work is supported by the National Natural Science Foundation of China (grants 41574157, 41322031, and 41628402) H. Zhang is partially supported by NSFAGS-1352669. M. D. Hartinger is supported by NASANNX17AD35G. I. J. Rae is supported by STFC grant ST/N000722/1, and NERC grants NE/L007495/1, NE/P017150/1, and NE/P017185/1. The work by YN and BW was supported by NSF grant PLR-1341359. Thanks to the NCAR High Altitude Observatory for hospitality to X. C. Shen. We are grateful to the International Space Science Institute-Beijing for supporting the international teams "Dayside Transient Phenomena and Their Impact on the Magnetosphere-Ionosphere" and "Multiple-instrument observations and simulations of the dynamical processes associated with polar cap patches/aurora and their associated scintillations".

References

Angelopoulos, V. (2008). The THEMIS mission. *Space Science Reviews*, *141*, 5–34.

Archer, M. O., Horbury, T. S., & Eastwood, J. P. (2012). Magnetosheath pressure pulses: Generation downstream of the bow shock from solar wind discontinuities. *Journal of Geophysical Research*, *117*, A05228. https://doi.org/10.1029/2011JA017468

Archer, M., Turner, D., Eastwood, J., Schwartz, S., & Horbury, T. (2015). Global impacts of a foreshock bubble: Magnetosheath, magnetopause and ground-based observations. *Planetary and Space Science*, *106*, 56–66.

Auster, H. U., Glassmeier, K. H., Magnes, W., Aydogar, O., Baumjohann, W., Constantinescu, D., et al. (2008). The THEMIS fluxgate magnetometer. *Space Science Reviews*, *141*, 235–264.

Berube, D., Moldwin, M., & Ahn, M. (2006). Computing magnetospheric mass density from field line resonances in a realistic magnetic field geometry. *Journal of Geophysical Research*, *111*, A08206. https://doi.org/10.1029/2005JA011450

Chen, L., & Hasegawa, A. (1974). A theory of long-period magnetic pulsations: 1. Steady state excitation of field line resonance. *Journal of Geophysical Research*, *79*(7), 1024–1032.

Claudepierre, S. G., Elkington, S. R., & Wiltberger, M. (2008). Solar wind driving of magnetospheric ULF waves: Pulsations driven by velocity shear at the magnetopause. *Journal of Geophysical Research*, *113*, A05218. https://doi.org/10.1029/2007JA012890

Claudepierre, S. G., Hudson, M. K., Lotko, W., Lyon, J. G., & Denton, R. E. (2010). Solar wind driving of magnetospheric ULF waves: Field line resonances driven by dynamic pressure fluctuations. *Journal of Geophysical Research*, *115*, A11202. https://doi.org/10.1029/2010JA015399

Degeling, A. W., Rankin, R., Kabin, K., Rae, I. J., & Fenrich, F. R. (2010). Modeling ULF waves in a compressed dipole magnetic field. *Journal of Geophysical Research*, *115*, A10212. https://doi.org/10.1029/2010JA015410

Denton, R., Goldstein, J., Lee, D.-H., King, R., Dent, Z., Gallagher, D., et al. (2006). Realistic magnetospheric density model for 29 August 2000. *Journal of Atmospheric and Solar-Terrestrial Physics*, *68*(6), 615–628.

Dmitriev, A., & Suvorova, A. (2015). Large-scale jets in the magnetosheath and plasma penetration across the magnetopause: THEMIS observations. *Journal of Geophysical Research: Space Physics*, *120*, 4423–4437. https://doi.org/10.1002/2014JA020953

Eastwood, J., Lucek, E., Mazelle, C., Meziane, K., Narita, Y., Pickett, J., & Treumann, R. (2005). The foreshock. *Space Science Reviews*, *118*(1–4), 41–94.

Eastwood, J., Schwartz, S., Horbury, T., Carr, C., Glassmeier, K.-H., Richter, I., et al. (2011). Transient Pc3 wave activity generated by a hot flow anomaly: Cluster, Rosetta, and ground-based observations. *Journal of Geophysical Research*, *116*, A08224. https://doi.org/10.1029/2011JA016467

Elkington, S. R., Hudson, M. K., & Chan, A. A. (1999). Acceleration of relativistic electrons via drift-resonant interaction with toroidal-mode Pc-5 ULF oscillations. *Geophysical Research Letters*, *26*(2), 3273–3276.

Hao, Y. X., Zong, Q. G., Zhou, X. Z., Rankin, R., Chen, X. R., Liu, Y., et al. (2017). Relativistic electron dynamics produced by azimuthally localized poloidal mode ULF waves: Boomerang-shaped pitch angle evolutions. *Geophysical Research Letters*, *44*, 7618–7627. https://doi.org/10.1002/2017GL074006

Hapgood, M., Lockwood, M., Bowe, G., Willis, D., & Tulunay, Y. (1991). Variability of the interplanetary medium at 1 AU over 24 years: 1963–1986. *Planetary and Space Science*, *39*(3), 411–423.

Hartinger, M., Angelopoulos, V., Moldwin, M. B., Glassmeier, K., & Nishimura, Y. (2011). Global energy transfer during a magnetospheric field line resonance. *Geophysical Research Letters*, *38*, L12101. https://doi.org/10.1029/2011GL047846

Hartinger, M., Turner, D., Plaschke, F., Angelopoulos, V., & Singer, H. (2013). The role of transient ion foreshock phenomena in driving Pc5 ULF wave activity. *Journal of Geophysical Research: Space Physics*, *118*, 299–312. https://doi.org/10.1029/2012JA018349

Hsu, T., & McPherron, R. L. (2007). A statistical study of the relation of Pi 2 and plasma flows in the tail. *Journal of Geophysical Research*, *112*, A05209. https://doi.org/10.1029/2006JA011782

Hudson, M. K., Elkington, S. R., Lyon, J. G., & Goodrich, C. C. (2000). Increase in relativistic electron flux in the inner magnetosphere: ULF wave mode structure. *Advances in Space Research*, *25*(1), 2327–2337.

Hudson, M., Jaynes, A., Kress, B. T., Li, Z., Patel, M., Shen, X.-C., et al. (2017). Simulated prompt acceleration of multi-MeV electrons by the 17 March 2015 interplanetary shock. *Journal of Geophysical Research: Space Physics*, *122*, 10,036–10,046. https://doi.org/10.1002/2017JA024445

Hughes, W. J. (2013). Magnetospheric ULF Waves: A Tutorial with a Historical Perspective. In M. J. Engebretson, K. Takahashi, & M. Scholer (Eds.), *Solar Wind Sources of Magnetospheric Ultra-Low-Frequency Waves*. https://doi.org/10.1029/GM081p0001

Jacobs, J. A., Kato, Y., Matsushita, S., & Troitskaya, V. A. (1964). Classification of geomagnetic micropulsations. *Geophysical Journal International*, *8*, 341–342.

Kepko, L, Spence, H. E., & Singer, H. J. (2002). ULF waves in the solar wind as direct drivers of magnetospheric pulsations. *Geophysical Research Letters*, *29*, 1197. https://doi.org/10.1029/2001GL014405

Lee, D.-H., & Lysak, R. L. (1989). Magnetospheric ULF wave coupling in the dipole model: The impulsive excitation. *Journal of Geophysical Research*, *94*(A12), 17,097–17,103.
McFadden, J. P., Carlson, C. W., Larson, D., Ludlam, M., Abiad, R., & Elliott, B. (2008). The THEMIS ESA plasma instrument and in-flight calibration. *Space Science Reviews*, *277–302*, 141.
Ogilvie, K. W., & Fitzenreiter, R. J. (1989). The Kelvin-Helmholtz instability at the magnetopause and inner boundary layer surface. *Journal of Geophysical Research*, *94*(A11), 15,113–15,123.
Olson, J. V. (1999). Pi2 pulsations and substorm onsets: A review. *Journal of Geophysical Research*, *A8*, 104.
Pu, Z., & Kivelson, M. G. (1983). Kelvin:Helmholtz instability at the magnetopause: Solution for compressible plasmas. *Journal of Geophysical Research*, *88*(A2), 841–852.
Rae, I. J., Murphy, K. R., Watt, C. E. J., Halford, A. J., Mann, I. R., Ozeke, L. G., et al. (2018). The role of localized compressional ultra-low frequency waves in energetic electron precipitation. *Journal of Geophysical Research: Space Physics*, *123*, 1900–1914. https://doi.org/10.1002/2017JA024674
Rankin, R., Kabin, K., Lu, J. Y., Mann, I. R., Marchand, R., Rae, I. J., et al. (2005). Magnetospheric field-line resonances: Ground-based observations and modeling. *Journal of Geophysical Research*, *110*, A10S09. https://doi.org/10.1029/2004JA010919
Sarris, T. E., Li, X., Liu, W., Argyriadis, E., Boudouridis, A., & Ergun, R. (2013). Mode number calculations of ULF field-line resonances using ground magnetometers and THEMIS measurements. *Journal of Geophysical Research: Space Physics*, *118*, 6986–6997. https://doi.org/10.1002/2012JA018307
Sarris, T. E., Liu, W., Kabin, K., Li, X., Elkington, S. R., Ergun, R., et al. (2009). Characterization of ULF pulsations by THEMIS. *Geophysical Research Letters*, *36*, L04104. https://doi.org/10.1029/2008GL036732
Sarris, T. E., Liu, W., Li, X. L., Kabin, K., Talaat, E. R., Rankin, R., et al. (2010). THEMIS observations of the spatial extent and pressure-pulse excitation of field line resonances. *Geophysical Research Letters*, *37*, L15104. https://doi.org/10.1029/2010GL044125
Savin, S., Amata, E., Zelenyi, L., Lutsenko, V., Safrankova, J., Nemecek, Z., et al. (2012). Super fast plasma streams as drivers of transient and anomalous magnetospheric dynamics. *Annales Geophysicae*, *30*(1), 1–7.
Shen, X., Shi, Q., Zong, Q.-G., Tian, A., Nowada, M., Sun, W., et al. (2017). Dayside magnetospheric ULF wave frequency modulated by a solar wind dynamic pressure negative impulse. *Journal of Geophysical Research: Space Physics*, *122*, 1658–1669. https://doi.org/10.1002/2016JA023351
Shen, X., Zong, Q.-G., Shi, Q., Tian, A., Sun, W., Wang, Y., et al. (2015). Magnetospheric ULF waves with increasing amplitude related to solar wind dynamic pressure changes: The time history of events and macroscale interactions during substorms (THEMIS) observations. *Journal of Geophysical Research: Space Physics*, *120*, 7179–7190. https://doi.org/10.1002/2014JA020913
Shi, Q. Q., Hartinger, M., Angelopoulos, V., Zong, Q., Zhou, X., Zhou, X., et al. (2013). THEMIS observations of ULF wave excitation in the nightside plasma sheet during sudden impulse events. *Journal of Geophysical Research: Space Physics*, *118*, 284–298. https://doi.org/10.1029/2012JA017984
Shi, Q. Q., Hartinger, M. D., Angelopoulos, V., Tian, A. M., Fu, S. Y., Zong, Q.-G., et al. (2014). Solar wind pressure pulse-driven magnetospheric vortices and their global consequences. *Journal of Geophysical Research: Space Physics*, *119*, 4274–4280. https://doi.org/10.1002/2013JA019551
Shue, J.-H., Song, P., Russell, C. T., Steinberg, J. T., Chao, J. K., Zastenker, G., et al. (1998). Magnetopause location under extreme solar wind conditions. *Journal of Geophysical Research*, *103*(A8), 17,691–17,700.
Sibeck, D., Borodkova, N., Schwartz, S., Owen, C., Kessel, R., Kokubun, S., et al. (1999). Comprehensive study of the magnetospheric response to a hot flow anomaly. *Journal of Geophysical Research*, *104*(A3), 4577–4593.
Southwood, D., Dungey, J., & Etherington, R. (1969). Bounce resonant interaction between pulsations and trapped particles. *Planetary and Space Science*, *17*, 349–361.
Takahashi, K., Hartinger, M. D., Angelopoulos, V., & Glassmeier, K.-H. (2015). A statistical study of fundamental toroidal mode standing Alfvén waves using THEMIS ion bulk velocity data. *Journal of Geophysical Research: Space Physics*, *120*, 6474–6495. https://doi.org/10.1002/2015JA021207
Takahashi, K., McEntire, R., Lui, A., & Potemra, T. (1990). Ion flux oscillations associated with a radially polarized transverse Pc 5 magnetic pulsation. *Journal of Geophysical Research*, *95*(A4), 3717–3731.
Tamao, T. (1965). Transmission and coupling resonance of hydromagnetic disturbances in the nonuniform Earth's magnetosphere. *Science Report Tohoku University, Fifth Series*, *17*, 43–72.
Tan, L. C., Fung, S. F., & Shao, X. (2004). Observation of magnetospheric relativistic electrons accelerated by Pc-5 ULF waves. *Geophysical Research Letters*, *31*, L14802. https://doi.org/10.1029/2004GL019459
Turner, D. L., Omidi, N., Sibeck, D. G., & Angelopoulos, V. (2013). First observations of foreshock bubbles upstream of Earth's bow shock: Characteristics and comparisons to HFAs. *Journal of Geophysical Research: Space Physics*, *118*, 1552–1570. https://doi.org/10.1002/jgra.50198
Turner, D. L., Shprits, Y., Hartinger, M., & Angelopoulos, V. (2012). Explaining sudden losses of outer radiation belt electrons during geomagnetic storms. *Nature Physics*, *8*(3), 208–212.
Walker, A., Greenwald, R., Korth, A., & Kremser, G. (1982). Stare and GEOS 2 observations of a storm time Pc 5 ULF pulsation. *Journal of Geophysical Research*, *87*(A11), 9135–9146.
Wang, B., Nishimura, Y., Hietala, H., Shen, X.-C., Shi, Q., Zhang, H., et al. (2018). Dayside magnetospheric and ionospheric responses to a fore-shock transient on June 25, 2008: 2.2-D evolution based on dayside auroral imaging. *Journal of Geophysical Research: Space Physics*, *123*. https://doi.org/10.1029/2017JA024846
Xiao, T., Zhang, H., Shi, Q., Zong, Q.-G., Fu, S. Y., Tian, A. M., et al. (2015). Propagation characteristics of young hot flow anomalies near the bow shock: Cluster observations. *Journal of Geophysical Research: Space Physics*, *120*, 4142–4154. https://doi.org/10.1002/2015JA021013
Zhang, H., Sibeck, D. G., Zong, Q.-G., Gary, S. P., McFadden, J. P., Larson, D., et al. (2010). Time history of events and macroscale interactions during substorms observations of a series of hot flow anomaly events. *Journal of Geophysical Research*, *115*, A12235. https://doi.org/10.1029/2009JA015180
Zhang, X. Y., Zong, Q.-G., Wang, Y. F., Zhang, H., Xie, L., Fu, S. Y., et al. (2010). ULF waves excited by negative/positive solar wind dynamic pressure impulses at geosynchronous orbit. *Journal of Geophysical Research*, *115*, A10221. https://doi.org/10.1029/2009JA015016
Zhao, L. L., Zhang, H., & Zong, Q. G. (2017). Global ULF waves generated by a hot flow anomaly. *Geophysical Research Letters*, *44*, 5283–5291. https://doi.org/10.1002/2017GL073249
Zong, Q.-G., Wang, Y. F., Zhang, H., Fu, S. Y., Zhang, H., Wang, C. R., et al. (2012). Fast acceleration of inner magnetospheric hydrogen and oxygen ions by shock induced ULF waves. *Journal of Geophysical Research*, *117*, A11206. https://doi.org/10.1029/2012JA018024
Zong, Q.-G., Zhou, X.-Z., Wang, Y. F., Li, X., Song, P., Baker, D. N., et al. (2009). Energetic electron response to ULF waves induced by interplanetary shocks in the outer radiation belt. *Journal of Geophysical Research*, *114*, A10204. https://doi.org/10.1029/2009JA014393